Electrocatalytic and Photocatalytic Hydrogen Production from Acidic and Neutral-pH Aqueous Solutions Using Iron Phosphide Nanoparticles

Juan F. Callejas,[†,§] Joshua M. McEnaney,[†,§] Carlos G. Read,[†,§] J. Chance Crompton,[‡] Adam J. Biacchi,[†] Eric J. Popczun,[†] Thomas R. Gordon,[†] Nathan S. Lewis,[*,‡] and Raymond E. Schaak[*,†]

[†]Department of Chemistry and Materials Research Institute, The Pennsylvania State University, University Park, Pennsylvania 16802, United States and [‡]Division of Chemistry and Chemical Engineering, California Institute of Technology, Pasadena, California 91125, United States. [§]These authors contributed equally.

ABSTRACT Nanostructured transition-metal phosphides have recently emerged as Earth-abundant alternatives to platinum for catalyzing the hydrogen-evolution reaction (HER), which is central to several clean energy technologies because it produces molecular hydrogen through the electrochemical reduction of water. Iron-based catalysts are very attractive targets because iron is the most abundant and least expensive transition metal. We report herein that iron phosphide (FeP), synthesized as nanoparticles having a uniform, hollow morphology, exhibits among the highest HER activities reported to date in both acidic and neutral-pH aqueous solutions. As an electrocatalyst operating at a current density of −10 mA cm^{-2}, FeP nanoparticles deposited at a mass loading of ∼1 mg cm^{-2} on Ti substrates exhibited overpotentials of −50 mV in 0.50 M H_2SO_4 and −102 mV in 1.0 M phosphate buffered saline. The FeP nanoparticles supported sustained hydrogen production with essentially quantitative faradaic yields for extended time periods under galvanostatic control. Under UV illumination in both acidic and neutral-pH solutions, FeP nanoparticles deposited on TiO_2 produced H_2 at rates and amounts that begin to approach those of Pt/TiO_2. FeP therefore is a highly Earth-abundant material for efficiently facilitating the HER both electrocatalytically and photocatalytically.

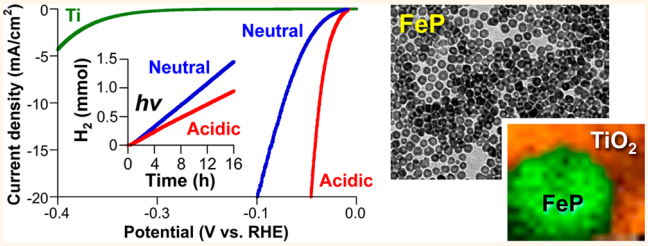

KEYWORDS: hydrogen evolution reaction · metal phosphides · nanoparticles · electrocatalysis · photocatalysis

Platinum is the most widely used material for the electrocatalytic and photocatalytic production of molecular hydrogen (H_2) from water through the hydrogen-evolution reaction (HER). Although Pt is highly active and stable under the often harsh operational conditions used in electrolyzers and photoelectrochemical cells,[1] Pt is expensive and scarce.[2] Hence, several new Earth-abundant HER catalysts have emerged, including MoS_2,[3,4] Ni−Mo,[5] $CoSe_2$,[6] CoS_2,[7] Ni_2P,[8,9] CoP,[10,11] MoP,[12,13] and WP,[14] as well as other related materials.[15−19] Iron-based alternatives are especially attractive because Fe is the most abundant transition metal, comprising ∼5% of the Earth's crust.[20] Accordingly, the price of iron is typically at least 2 orders of magnitude less than that of other highly abundant and catalytically relevant metals for the HER, including Ni and Co.[20] Iron-based clusters also have been found to be the catalytically active sites in [FeFe] and [Fe]-only hydrogenases, which are highly active and efficient biological HER catalysts.[21] A few moderately active iron-based heterogeneous HER catalysts have been reported, including porous FeP nanosheets,[22] pyrrhotite-type FeS nanoparticles,[23] and polycrystalline films of pyrite-type FeS_2.[16] However, highly active HER catalysts composed of high-quality iron-based nanoparticulate materials, which are among the most desired because of their cost, abundance, and processability, have not yet been identified.

We report herein that iron phosphide (FeP) nanoparticles are exceptionally active as both electrocatalysts and photocatalysts for sustained hydrogen production in either

* Address correspondence to schaak@chem.psu.edu, nslewis@caltech.edu.

Received for review August 28, 2014 and accepted September 24, 2014.

Published online September 24, 2014
10.1021/nn5048553

acidic or neutral-pH aqueous solutions. With overpotentials of −50 mV in 0.50 M H_2SO_4 and −102 mV in 1.0 M phosphate buffered saline (PBS), respectively, both at an operationally relevant current density of −10 mA cm^{-2}, FeP outperforms comparable, previously reported non-noble metal nanoparticle HER electrocatalysts in both acidic and neutral-pH aqueous solutions. In addition, when immobilized on TiO_2, the FeP nanoparticles effect the photocatalytic generation of hydrogen under UV irradiation in acidic and neutral-pH aqueous solutions, making FeP/TiO_2 a fully Earth-abundant system for sustained photocatalytic hydrogen production. This high electrocatalytic and photocatalytic activity, coupled with the high terrestrial abundance and low cost of its constituent elements, makes FeP an important addition to the growing family of transition-metal phosphide nanostructures that have been identified as active HER catalysts.

RESULTS AND DISCUSSION

To synthesize the FeP nanoparticles, Fe nanoparticles were prepared by decomposing $Fe(CO)_5$ in a mixture of oleylamine and 1-octadecene at 190 °C, followed by reaction with trioctylphosphine (TOP) at 340 °C for 1 h. This procedure is modified from a previous report.[24] Transmission electron microscopy (TEM) images (Figure 1) indicated the formation of spherical, hollow particles with an average diameter of 13 ± 2 nm. The corresponding high-resolution TEM (HRTEM) image (Figure 1b) revealed that the hollow particles were single crystalline and faceted and are therefore morphologically similar to other transition-metal phosphide nanoparticles formed by chemically transforming metal seed particles into phosphides using TOP.[8,10] The lattice fringes observed by HRTEM were 2.9 and 2.6 Å, which corresponded well to the (002) and (200) planes of MnP-type FeP, respectively.

The powder X-ray diffraction (XRD) pattern for the product corresponded well with that expected for nanocrystalline MnP-type FeP (Figure 2a). Scherrer analysis of the peak widths indicated an average grain size of 11 nm, which is consistent with the average particle size observed by TEM and suggests that the nanocrystalline particles observed by TEM comprise the bulk of the sample. A selected area electron diffraction (SAED) pattern acquired from an ensemble of particles (Figure 2b) exhibited rings that were fully indexed to MnP-type FeP, consistent with the bulk XRD data. The energy-dispersive X-ray spectroscopy (EDS) data (Supporting Information Figure S1) indicated an Fe/P ratio of 44:56, which is consistent with the expected FeP stoichiometry, along with a slight excess of P that is likely due to surface-bound TOP.

Working electrodes with FeP nanoparticle mass loadings of 1 mg cm^{-2} on Ti substrates were heated for 2 h at 450 °C in H_2(5%)/Ar(95%) to remove the surface ligands (Figure S2). The electrocatalytic HER

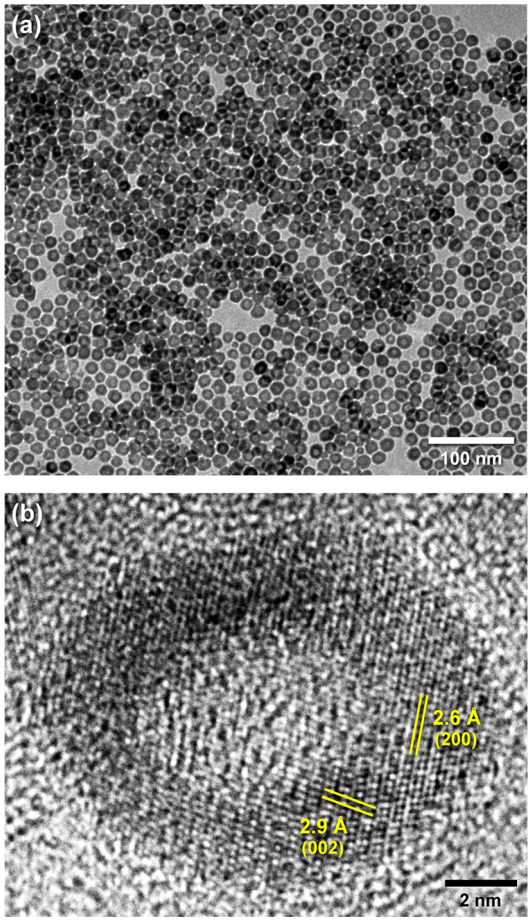

Figure 1. (a) TEM and (b) HRTEM image of the FeP nanoparticles.

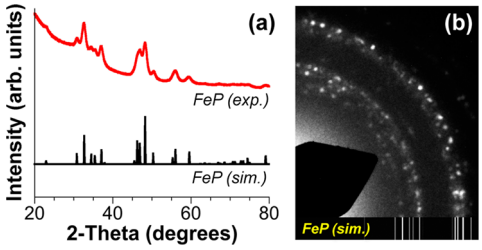

Figure 2. (a) Powder XRD data and (b) SAED pattern for the FeP nanoparticles. Both simulated and experimental XRD and SAED data are shown for comparison.

activity was then evaluated in acidic [0.50 M H_2SO_4] and neutral-pH [1.0 M PBS] aqueous solutions. No Pt contamination was detectable by X-ray photoelectron spectroscopy (XPS). Figure 3 shows polarization (current density *vs* potential) data for three individual FeP/Ti electrodes, along with data for Ti, which is not an active HER catalyst, as well as data for Pt, which is a benchmark HER catalyst. In acidic solutions, the FeP/Ti electrodes produced current densities of −10 and −20 mA cm^{-2} at overpotentials of −50 and −61 mV, respectively (*i.e.*, $\eta_{-10\ mA/cm^2}$ = −50 mV and $\eta_{-20\ mA/cm^2}$ = −61 mV). These overpotentials approached those of the Pt electrode

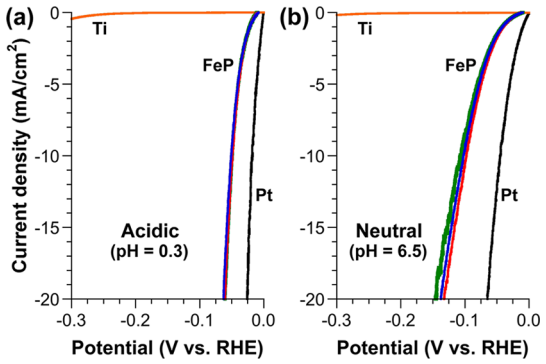

Figure 3. Polarization data for three distinct FeP/Ti electrodes, along with Pt and Ti, in (a) 0.50 M H_2SO_4 and (b) 1.0 M PBS.

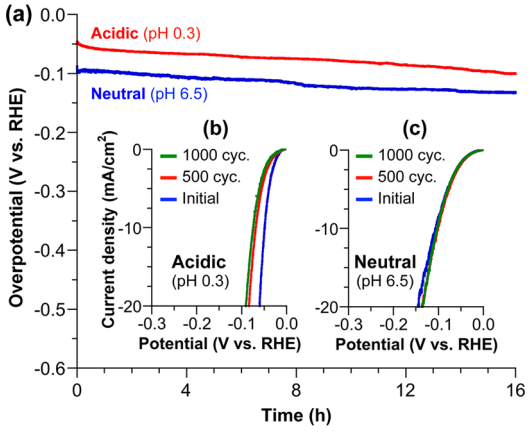

Figure 4. Plots for FeP/Ti electrodes in 0.50 M H_2SO_4 and 1.0 M PBS, respectively, of (a) overpotential *vs* time and (b,c) current density *vs* potential, initially and after 500 and 1000 CV sweeps between +0.1 and −0.15 V *vs* RHE.

($\eta_{-10\ mA/cm^2} = -18$ mV and $\eta_{-20\ mA/cm^2} = -26$ mV) and are lower than those of other relevant and comparable systems in acidic solutions tested under identical conditions, including Ni_2P ($\eta_{-20\ mA/cm^2} = -130$ mV)[8] and CoP ($\eta_{-20\ mA/cm^2} = -85$ mV).[10] Previously reported overpotentials at comparable current densities and mass loadings suggest that the electrocatalytic HER activity of the FeP/Ti electrodes also compares favorably to that of other relevant systems, including $CoSe_2$ ($\eta_{-20\ mA/cm^2} = -150$ mV),[6] CoS_2 ($\eta_{-20\ mA/cm^2} = -162$ mV),[7] MoS_2/RGO ($\eta_{-20\ mA/cm^2} = -185$ mV),[4] polycrystalline films of pyrite-type FeS_2 ($\eta_{-10\ mA/cm^2} = -265$ mV),[16] and porous FeP nanosheets ($\eta_{-20\ mA/cm^2} = -325$ mV).[22] The enhanced activity of our FeP nanoparticles relative to the HER activity of porous FeP nanosheets previously reported may be due in part to the increased accessible surface area produced by the small particle sizes, in conjunction with ligand removal *via* thermal annealing, as well as other intrinsic factors that include crystallinity and phase purity.

The FeP/Ti electrodes also functioned as highly active HER electrocatalysts in neutral-pH aqueous solutions, with $\eta_{-10\ mA/cm^2} = -102$ mV and $\eta_{-20\ mA/cm^2} = -136$ mV. For comparison, Pt exhibited a high HER activity, as expected ($\eta_{-10\ mA/cm^2} = -45$ mV and $\eta_{-20\ mA/cm^2} = -65$ mV), while the bare Ti foil exhibited large overpotentials. While less active than in acidic solutions, these overpotential values in neutral-pH solutions are comparable to those of CoP nanowire arrays ($\eta_{-10\ mA/cm^2} = -106$ mA)[11] and compare favorably to other related systems, including Mo_2C ($\eta_{-1\ mA/cm^2} = -200$ mV),[17] MoB ($\eta_{-1\ mA/cm^2} = -250$ mV),[17] pyrrhotite-type FeS nanoparticles ($\eta_{-0.7\ mA/cm^2} = -450$ mV),[23] and Co-embedded nitrogen-doped carbon nanotubes ($\eta_{-10\ mA/cm^2} = -540$ mV).[25]

For the Pt electrode in 0.50 M H_2SO_4, the slope of the Tafel plot [overpotential *vs* log(current density)] was ~30 mV/decade, with an exchange current density of 2.49×10^{-3} A cm^{-2} (Figure S3). Both values are consistent with the known behavior of Pt for the HER.[8,10] For the FeP/Ti electrodes in 0.50 M H_2SO_4, Tafel analysis yielded a slope of ~37 mV/decade. The FeP Tafel slope is comparable to Tafel slopes for related systems such as MoS_2 on reduced graphene oxide (41 mV/decade),[4] $CoSe_2$ (42 mV/decade),[6] and Co-embedded nitrogen-doped carbon nanotubes (42 mV/decade)[25] and is significantly lower than the Tafel slopes for Ni_2P (46 mV/decade)[8] and CoP (50 mV/decade).[10] The exchange current density for FeP/Ti in acidic solutions was 4.3×10^{-4} A cm^{-2}, consistent with the high activity of FeP and intermediate between that of the Pt control (2.49×10^{-3} A cm^{-2}) and Ni_2P (3.3×10^{-5} A cm^{-2}).[8] The turnover frequency (TOF) in 0.50 M H_2SO_4 at $\eta = 100$ mV was estimated to be 0.277 s^{-1}, which is comparable to previous reports for related systems.[8−11] The faradaic efficiencies of both an FeP/Ti electrode and the Pt control were determined by maintaining a current of −10 mA for 50 min, thus passing 30 C of charge. The amount of H_2 collected was consistent with that expected based on the amount of charge passed through the system, indicating a quantitative faradaic yield. (See Supporting Information for details of all analyses and calculations.)

The stabilities of the FeP/Ti electrodes in acidic and neutral solutions were first evaluated under galvanostatic conditions at a current density of −10 mA cm^{-2} for 16 h. Over this time period, the overpotentials increased by approximately 52 mV in acidic solutions but by only ~35 mV in neutral-pH solutions (Figure 4a). Accelerated degradation studies were also performed using cyclic voltammetry (CV), in which the FeP/Ti electrodes were cycled between +0.1 and −0.15 V *vs* RHE (reversible hydrogen electrode). After 500 and 1000 cycles, the overpotential in acidic solutions increased by approximately 19 and 25 mV, respectively (Figure 4b). Several factors could lead to such overpotential increases during CV cycling and galvanostatic testing in 0.50 M H_2SO_4, including sample degradation and the formation of surface oxides.

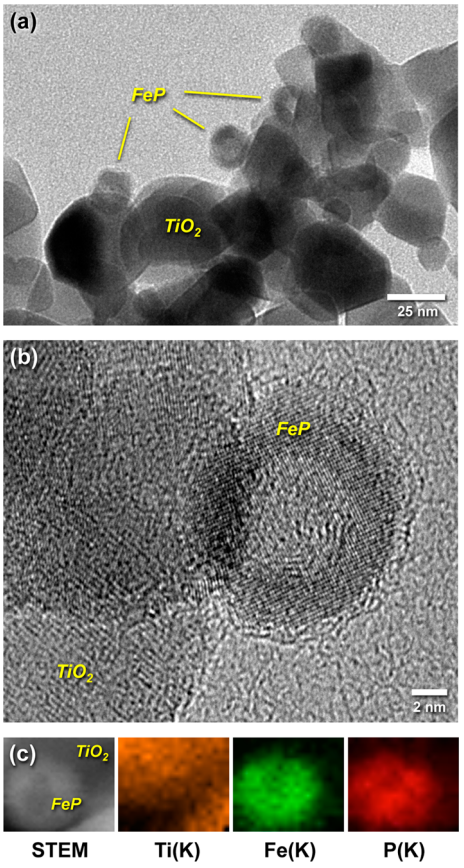

Figure 5. (a) TEM image, (b) HRTEM image, and (c) STEM-EDS element maps of the FeP/TiO_2 nanocomposite.

XRD data for the FeP/Ti electrodes after 500 and 1000 cycles in 0.50 M H_2SO_4 confirmed that the nanocrystalline MnP-type FeP phase persisted. Notably, the analogous CV cycling experiments and galvanostatic testing in 1.0 M PBS showed no measurable increase in overpotential (Figure 4c), indicating that the FeP particles were very stable under neutral-pH conditions.

In addition to serving as an efficient HER electrocatalyst, FeP nanoparticles immobilized on TiO_2 photocatalytically generated hydrogen under UV illumination in acidic and neutral-pH aqueous solutions. For this purpose, the FeP nanoparticles were adsorbed onto Degussa P25 TiO_2 using a literature protocol, which includes annealing at 450 °C under H_2(5%)/Ar(95%).[26] A TEM image of the FeP/TiO_2 sample (Figure 5a), along with a corresponding HRTEM image (Figure 5b) and STEM-EDS element map (Figure 5c), confirmed that the FeP nanoparticles remained unchanged in morphology, uniformity, composition, and phase after deposition onto the TiO_2, although a putative carbonaceous shell might be formed during the annealing process.

Photocatalysis was performed under UV illumination provided by a 200 W Hg(Xe) arc lamp that was fitted with a water filter to cut off the infrared radiation. (See Figure S4 and the Supporting Information for details.) Methanol (MeOH) was used as a sacrificial electron donor, and the gaseous reaction products were monitored at 10 min intervals by an online gas chromatograph (GC) with a thermal conductivity detector. Figures 6a,b and S5 show the rates of H_2 production as well as the total amounts of H_2 produced as a function of time under acidic [50:50 MeOH/HCl(1 M)] and neutral-pH [50:50 MeOH/H_2O] conditions for FeP/TiO_2, as well as for Pt/TiO_2 and TiO_2. All cocatalyst mass loadings were 1.5 wt %, as confirmed by atomic absorption spectroscopy. The TiO_2-supported FeP nanoparticles exhibited sustained photocatalytic H_2 production over 16 h with minimal decrease in activity under both acidic and neutral-pH conditions. After testing, the FeP/TiO_2 composite remained largely intact (Figure S6). Bare TiO_2 is a relatively inactive photocatalyst for hydrogen production, and indeed, TiO_2 alone showed a negligible rate of H_2 production. Consistently, the Pt/TiO_2 control was highly active for H_2 production, yielding average rates of 4.7 and 3.5 μmol H_2 mg^{-1} h^{-1} in acidic and neutral-pH solutions, respectively. The average rates of H_2 production for FeP/TiO_2 were 1.2 and 1.9 μmol H_2 mg^{-1} h^{-1} in acidic and neutral-pH solutions, respectively. The apparent quantum yields were 0.056 and 0.087 in acidic and neutral solutions, respectively, and were comparable to the quantum yields observed for related nonnoble metal HER catalyst systems.[27] Notably, and in contrast to the Pt/TiO_2 control, FeP/TiO_2 was slightly more active under neutral-pH conditions than under acidic conditions.

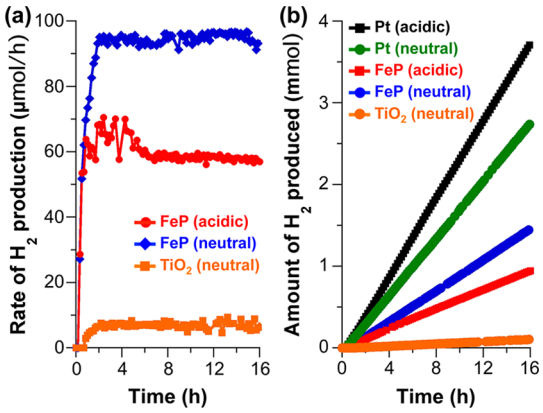

Figure 6. Plots of (a) H_2 production rate *vs* time and (b) amount of H_2 produced *vs* time in acidic and neutral solutions using the FeP/TiO_2 nanocomposite and UV illumination, as described in the text.

CONCLUSIONS

In summary, FeP nanoparticles, as an Earth-abundant system, exhibit exceptionally high activity for electrocatalytic and photocatalytic H_2 production in both acidic and neutral-pH aqueous solutions. The observed overpotentials of −50 and −102 mV to produce current densities of −10 mA cm^{-2} in 0.50 M H_2SO_4 and 1.0 M PBS, respectively, place FeP among

the most active non-noble metal HER electrocatalysts reported to date. The FeP nanoparticles are substantially more active than previously reported iron-based materials and are highly desirable non-Pt systems for global scalability because of the exceptionally high Earth abundance and low cost of Fe. Accordingly, FeP/TiO_2 was shown to comprise a fully Earth-abundant system for the sustained photocatalytic production of H_2(g) from both acidic and neutral-pH aqueous solutions.

MATERIALS AND METHODS

Chemicals and Materials. Octadecene [90%, $C_{18}H_{36}$, Sigma-Aldrich], oleylamine [70%, $C_{18}H_{37}N$, Sigma-Aldrich], oleic acid [technical grade, 90%, Sigma-Aldrich], pentacarbonyliron [99.5%, $Fe(CO)_5$, Alfa-Aesar], squalane [98%, $C_{30}H_{62}$, Alfa-Aesar], tri-*n*-octylphosphine [>85%, $P(C_8H_{16})_3$, TCI America], platinum(II) 2,4-pentanedionate [Pt 48.0% min, Alfa-Aesar], titanium foil [99.7%, 0.25 mm thickness], potassium phosphate dibasic [>98%, K_2HPO_4, Sigma-Aldrich], sodium phosphate monobasic [>98%, NaH_2PO_4, Sigma-Aldrich], hydrochloric acid [37%, Sigma-Aldrich], sulfuric acid [99.999%, Sigma-Aldrich], and methanol [technical grade] were used as received. High-quality colloidal Ag paint was purchased from SPI Supplies, and two-part epoxy [HYSOL 9460] was purchased from McMaster-Carr. Degussa P25 TiO_2 [Aeroxide P25 titanium(IV) oxide nanopowder, 21 nm particle size (TEM), ≥99.5% trace metals basis] was purchased from Sigma-Aldrich, and 1.0 M PBS solution, with a measured pH of 6.5, was made by dissolving 69 g of $NaH_2PO_4 \cdot H_2O$ (0.5 mol) and 71 g of Na_2HPO_4 (0.5 mol) in 1 L of water obtained from a Barnsted Nanopure column.

Synthesis of Hollow Iron Phosphide Nanoparticles. [*Caution:* This reaction should be considered to be highly corrosive and flammable because the high-temperature decomposition of a phosphine can liberate phosphorus, which is pyrophoric. Therefore, this reaction should only be carried out using rigorously air-free conditions by appropriately trained personnel.] Hollow iron phosphide nanoparticles were synthesized from colloidal iron nanoparticles by slightly modifying a previously reported process.[24] 1-Octadecene (ODE, 10.0 mL, 31.3 mmol) and oleylamine (0.2 mL, 0.61 mmol) were added to a 50 mL, three-necked, round-bottom flask that was equipped with a reflux condenser, a thermometer adapter, a thermometer, a rubber septum, and a borosilicate-coated stir bar. The contents of the flask were stirred and heated to 120 °C under vacuum for 30 min to remove any adventitious water and then placed under an Ar atmosphere. This ODE/oleylamine solution was then heated to 190 °C, at which point 0.35 mL of pentacarbonyliron was injected. The suspension was then maintained at 190 °C for 20 min. Five milliliters of the hot ODE/oleylamine mixture, which at this point now contained colloidal Fe nanoparticles, was then rapidly injected (using a glass syringe) into a second Ar-filled 50 mL, three-necked flask containing squalane (7.0 mL, 13 mmol) and tri-*n*-octylphosphine (3.0 mL, 6.7 mmol) that had been heated to 340 °C for 1 h. The temperature dropped as a result of the injection and was brought back up to 320 °C and held at that temperature for 1 h. After the reaction was completed, the heating mantle was turned off and the solution was allowed to cool to 200 °C. The heating mantle was then removed to allow the sample to cool more rapidly to room temperature. The reaction solution was divided into two centrifuge tubes for collection and cleaning. The nanoparticles were collected by adding hexanes (5 mL) and ethanol (15 mL) to each tube, followed by centrifugation (12 000 rpm, 3 min). The particles were then resuspended in hexanes (5 mL), and this process was repeated twice more. Nanoparticles were redispersed in hexanes after isolation and placed in a vial (20 mL) for use.

Preparation of Working Electrodes. Electrode fabrication was analogous to that described in previous reports.[8,10,12,14] FeP nanoparticles were deposited onto 0.2 cm^2 pieces of Ti foil using 5 μL increments of a 10 mg mL^{-1} solution, up to a total of 20 μL. After drying, the FeP/Ti foils were heated at 450 °C in H_2(5%)/Ar(95%) and were then attached to a polyvinyl chloride-coated Cu wire. A two-part epoxy was used to insulate the conductive surfaces, with the exception of the FeP-decorated side of the Ti foil.

Electrochemical Measurements. Electrochemical measurements were acquired using a Gamry Instruments Reference 600 potentiostat and were performed in 1.0 M phosphate buffered saline when testing in neutral-pH conditions or in 0.50 M H_2SO_4 when testing in acidic conditions. Current Interrupt (built into the potentiostat) was used to account for uncompensated solution resistance in all measurements. A three-electrode cell with two compartments was used, and the compartments were separated by a Nafion membrane (Fuelcellstore.com) to inhibit contamination of the working electrode by the contents of the counter electrode solution. A mercury/mercurous sulfate (Hg/Hg_2SO_4) electrode was used as the reference electrode, and a Pt mesh electrode was used as the counter electrode. Polarization data were acquired at a sweep rate of 1 mV s^{-1} while research-grade H_2(g) was continuously bubbled through the solution, which was rapidly stirred with a magnetic stir bar. Measurement of the open-circuit potential of a clean Pt mesh electrode in the electrolyte solution allowed for the determination of the RHE potential after the electrochemical characterization of iron phosphide. An initial measure of electrochemical stability was obtained by holding the current density galvanostatically at 10 mA cm^{-2} for 16 h. Long-term electrochemical stability was simulated using cyclic voltammetric sweeps between +0.1 and −0.15 V *vs* RHE at 100 mV s^{-1}. Turnover frequencies were estimated as reported previously.[8,10]

Quantitative Hydrogen Yield Measurements. Hydrogen yield measurements were performed in both the acidic and neutral solutions using a two-electrode, single-compartment cell. Graphitic carbon was used as the counter electrode with either FeP/Ti or Pt as the working electrode. The evolved H_2(g) was captured *via* an inverted graduated cylinder, positioned above the working electrode, which contained the electrolyte solution. In each experiment, a cathodic current of 10 mA was passed continuously through the 0.2 cm^2 working electrode over a 50 min (3000 s) duration, resulting in 30 C of total cathodic charge passed. For both acidic and neutral conditions, the FeP/Ti electrodes produced a volume of H_2(g) that was equivalent to the volume collected above Pt nanoparticle electrodes. All experiments yielded 3.96 ± 0.03 mL of hydrogen. This is comparable to the faradaic theoretical H_2 yield of 3.74 mL calculated at 1 atm and 20 °C (ambient conditions) for 30 C of charge.

Synthesis of Pt Nanoparticles. The Pt nanoparticles were synthesized using an adaptation of a previously reported procedure.[28] In the synthesis, 100 mg of $Pt(acac)_2$, 10 mL of ODE, 1 mL of OLAC, and 1 mL of OLAM were added to a 50 mL, three-necked, round-bottomed flask fitted with a condenser, magnetic stir bar, thermometer adapter, thermometer, and rubber septum at room temperature. The mixture was stirred under vacuum at ~120 °C for 20 min to remove any adventitious oxygen and water. The reaction was then placed under Ar and heated to 185 °C, and 0.1 mL of a previously prepared $Fe(CO)_5$ solution (0.75 M in ODE) was then quickly injected. The reaction proceeded at a temperature of 200 °C for 20 min. The Pt nanoparticle product, which was previously found to not contain observable Fe at the surface,[28] was then cooled to room temperature by removing the flask from the heating mantle and subsequently transferring the suspension to centrifuge tubes. Ethanol was added to the tubes (1:1 by volume), and the product was centrifuged at 10 000 rpm for 5 min. The black precipitate was redispersed in hexanes and ethanol (1:1 by volume) and centrifuged at 10 000 rpm. The product was then redispersed in hexanes and stored.

Preparation of Pt/TiO_2 and FeP/TiO_2. The Pt and FeP nanoparticles were anchored onto Degussa P25 TiO_2 using an adaptation of a previously reported procedure.[26] A toluene solution of Pt or FeP nanoparticles of the appropriate concentration was added to a dispersion of TiO_2 in toluene. After being stirred for 1 h, the solid was separated by centrifugation and washed with acetone, along with the use of mild sonication. The obtained slurry was then vacuum-dried and heated for 2.5 h at 450 °C under a H_2(5%)/Ar(95%) atmosphere to remove the surface ligands and to ensure the formation of a robust solid−solid interface between the nanoparticles and the TiO_2 support. The Pt/TiO_2 sample was annealed for 3 h in air at 350 °C.

Photocatalytic Testing. Approximately 50 mg of Pt/TiO_2 or FeP/TiO_2 was suspended with sonication in 50 mL of a 1:1 MeOH/H_2O solution (pH-neutral solution) or 1 M HCl (acidic solution). Prior to the tests, the reactor was purged with Ar for ~25 min to ensure the removal of air. An Ar flow of 10 mL min^{-1} was maintained during testing. UV illumination was provided by a 200 W Hg(Xe) arc lamp fitted with a water filter to cut off the infrared radiation. Using a Newport OSM-400 spectrophotometer, the power density at the surface of the sample was measured to be ~5.6 mW/cm^2 over wavelengths shorter than 365 nm, which corresponds to a photon flux of $\sim 3.65 \times 10^{17}$ photons/s. The gaseous reaction products were monitored at 10 min intervals by an online gas chromatograph (Shimadzu GC-2014) equipped with a thermal conductivity detector.

Materials Characterization. Powder X-ray diffraction patterns were acquired using a Bruker-AXS D8 Advance diffractometer with Cu Kα radiation and a LynxEye 1-D detector. The CrystalMaker/CrystalDiffract software package was used to simulate XRD patterns for MnP-type FeP. Microscopy samples were prepared by drop-casting 0.7 μL of dispersed FeP in hexanes onto a 400 mesh Formvar and carbon-coated Cu grid (Electron Microscopy Sciences). Transmission electron microscopy images were obtained using a JEOL 1200 microscope that was operated at an accelerating voltage of 80 kV. A JEOL JEM-2010F microscope equipped with an EDAX solid-state X-ray detector was used to collect high-resolution TEM images at an accelerating voltage of 200 kV, as well as scanning transmission electron microscopy (STEM) images and energy-dispersive X-ray spectroscopy data. ES Vision software (Emispec) was used for EDS and STEM-EDS data processing, with the Fe K-shell and P K-shell transitions chosen for quantitative EDS analysis. XPS analysis was performed on a monochromatic Al Kα source Kratos Axis Ultra operating at 14 kV and 20 mA for an X-ray power of 280 W. XPS spectra were acquired with a photoelectron takeoff angle of 90° from the sample surface plane and were referenced to the C_{1s} peak with a binding energy of 285 eV. Diffuse reflectance infrared Fourier transform (DRIFT) spectra were acquired using a Bruker IFS 66/s spectrometer (Bruker Optics, Billerica, MA). KBr powder was used to dilute the nanoparticle samples for analysis, and DRIFT spectra were processed with OPUS 6.0 (Bruker Optics, Billerica, MA). The catalyst loadings on TiO_2 were verified using a Shimadzu AA-7000 atomic absorption spectrophotometer.

Conflict of Interest: The authors declare no competing financial interest.

Acknowledgment. The work at PSU was supported by the National Science Foundation (NSF) Center for Chemical Innovation on Solar Fuels (CHE-1305124) and at Caltech by the Joint Center for Artificial Photosynthesis, a DOE Energy Innovation Hub, supported through the Office of Science of the U.S. Department of Energy under Award Number DE-SC0004993. TEM was performed in the Penn State Microscopy and Cytometry Facility (University Park, PA), and HRTEM, EDS, XPS, and DRIFTS data were acquired at the Materials Characterization Laboratory of the Penn State Materials Research Institute. The authors thank Greg Barber, Jennifer Gray, Lymaris Ortiz Rivera, and Nella Vargas-Barbosa for technical support and helpful discussions.

Supporting Information Available: Complete experimental details and additional characterization data. This material is available free of charge *via* the Internet at http://pubs.acs.org.

REFERENCES AND NOTES

1. Walter, M. G.; Warren, E. L.; McKone, J. R.; Boettcher, S. W.; Mi, Q. X.; Santori, E. A.; Lewis, N. S. Solar Water Splitting Cells. *Chem. Rev.* **2010**, *110*, 6446–6473.
2. Gray, H. B. Powering the Planet with Solar Fuel. *Nat. Chem.* **2009**, *1*, 7.
3. Hinnemann, B.; Moses, P. G.; Bonde, J.; Jørgensen, K. P.; Nielsen, J. H.; Horch, S.; Chorkendorff, I.; Nørskov, J. K. Biomimetic Hydrogen Evolution: MoS_2 Nanoparticles as Catalyst for Hydrogen Evolution. *J. Am. Chem. Soc.* **2005**, *127*, 5308–5309.
4. Li, Y.; Wang, H.; Xie, L.; Liang, Y.; Hong, G.; Dai, H. MoS_2 Nanoparticles Grown on Graphene: An Advanced Catalyst for the Hydrogen Evolution Reaction. *J. Am. Chem. Soc.* **2011**, *133*, 7296–7299.
5. Raj, I. A.; Vasu, K. I. Transition Metal-Based Hydrogen Electrodes in Alkaline Solution—Electrocatalysis on Nickel Based Binary Alloy Coatings. *J. Appl. Electrochem.* **1990**, *20*, 32–38.
6. Kong, D. S.; Wang, H. T.; Lu, Z. Y.; Cui, Y. $CoSe_2$ Nanoparticles Grown on Carbon Fiber Paper: An Efficient and Stable Electrocatalyst for Hydrogen Evolution Reaction. *J. Am. Chem. Soc.* **2014**, *136*, 4897–4900.
7. Faber, M. S.; Dziedzic, R.; Lukowski, M. A.; Kaiser, N. S.; Ding, Q.; Jin, S. High-Performance Electrocatalysis Using Metallic Cobalt Pyrite (CoS_2) Micro- and Nanostructures. *J. Am. Chem. Soc.* **2014**, *136*, 10053–10061.
8. Popczun, E. J.; McKone, J. R.; Read, C. G.; Biacchi, A. J.; Wiltrout, A. M.; Lewis, N. S.; Schaak, R. E. Nanostructured Nickel Phosphide as an Electrocatalyst for the Hydrogen Evolution Reaction. *J. Am. Chem. Soc.* **2013**, *135*, 9267–9270.
9. Feng, L.; Vrubel, H.; Bensimon, M.; Hu, X. Easily-Prepared Dinickel Phosphide (Ni_2P) Nanoparticles as an Efficient and Robust Electrocatalyst for Hydrogen Evolution. *Phys. Chem. Chem. Phys.* **2014**, *16*, 5917–5921.
10. Popczun, E. J.; Read, C. G.; Roske, C. W.; Lewis, N. S.; Schaak, R. E. Highly Active Electrocatalysis of the Hydrogen Evolution Reaction by Cobalt Phosphide Nanoparticles. *Angew. Chem., Int. Ed.* **2014**, *53*, 5427–5430.
11. Tian, J. Q.; Liu, Q.; Asiri, A. M.; Sun, X. P. Self-Supported Nanoporous Cobalt Phosphide Nanowire Arrays: An Efficient 3D Hydrogen-Evolving Cathode over the Wide Range of pH 0−14. *J. Am. Chem. Soc.* **2014**, *136*, 7587–7590.
12. McEnaney, J. M.; Crompton, J. C.; Callejas, J. F.; Popczun, E. J.; Biacchi, A. J.; Lewis, N. S.; Schaak, R. E. Amorphous Molybdenum Phosphide Nanoparticles for Electrocatalytic Hydrogen Evolution. *Chem. Mater.* **2014**, *26*, 4826–4831.
13. Xiao, P.; Sk, M. A.; Thia, L.; Ge, X.; Lim, R. J.; Wang, J.-Y.; Lim, K. H.; Wang, X. Molybdenum Phosphide as an Efficient Electrocatalyst for the Hydrogen Evolution Reaction. *Energy Environ. Sci.* **2014**, *7*, 2624–2629.
14. McEnaney, J. M.; Crompton, J. C.; Callejas, J. F.; Popczun, E. J.; Read, C. G.; Lewis, N. S.; Schaak, R. E. Electrocatalytic Hydrogen Evolution Using Amorphous Tungsten Phosphide Nanoparticles. *Chem. Commun.* **2014**, *50*, 11026–11028.
15. Huang, Z.; Chen, Z.; Chen, Z.; Lv, C.; Meng, H.; Zhang, C. $Ni_{12}P_5$ Nanoparticles as an Efficient Catalyst for Hydrogen Generation *via* Electrolysis and Photoelectrolysis. *ACS Nano* **2014**, *8*, 8121–8129.
16. Kong, D. S.; Cha, J. J.; Wang, H. T.; Lee, H. R.; Cui, Y. First-Row Transition Metal Dichalcogenide Catalysts for Hydrogen Evolution Reaction. *Energy Environ. Sci.* **2013**, *6*, 3553–3558.
17. Vrubel, H.; Hu, X. L. Molybdenum Boride and Carbide Catalyze Hydrogen Evolution in Both Acidic and Basic Solutions. *Angew. Chem., Int. Ed.* **2012**, *51*, 12703–12706.
18. Chen, W. F.; Muckerman, J. T.; Fujita, E. Recent Developments in Transition Metal Carbides and Nitrides as Hydrogen Evolution Electrocatalysts. *Chem. Commun.* **2013**, *49*, 8896–8909.
19. Cao, B.; Veith, G. M.; Neuefeind, J. C.; Adzic, R. R.; Khalifah, P. G. Mixed Close-Packed Cobalt Molybdenum Nitrides as

Non-noble Metal Electrocatalysts for the Hydrogen Evolution Reaction. *J. Am. Chem. Soc.* **2013**, *135*, 19186–19192.
20. U.S. Geological Survey, Metal Prices in the United States through 2010: U.S. Geological Survey Scientific Investigations Report 2012-5188, 2013, http://pubs.usgs.gov/sir/2012/5188/ (accessed August 25, 2014).
21. Shima, S.; Pilak, O.; Vogt, S.; Schick, M.; Stagni, M. S.; Meyer-Klaucke, W.; Warkentin, E.; Thauer, R. K.; Ermler, U. The Crystal Structure of [Fe]-Hydrogenase Reveals the Geometry of the Active Site. *Science* **2008**, *321*, 572–575.
22. Xu, Y.; Wu, R.; Zhang, J.; Shi, Y.; Zhang, B. Anion-Exchange Synthesis of Nanoporous FeP Nanosheets as Electrocatalysts for Hydrogen Evolution Reaction. *Chem. Commun.* **2013**, *49*, 6656–6658.
23. Di Giovanni, C.; Wang, W.-A.; Nowak, S.; Grenèche, J.-M.; Lecoq, H.; Mouton, L.; Giraud, M.; Tard, C. Bioinspired Iron Sulfide Nanoparticles for Cheap and Long-Lived Electrocatalytic Molecular Hydrogen Evolution in Neutral Water. *ACS Catal.* **2014**, *4*, 681–687.
24. Muthuswamy, E.; Kharel, P. R.; Lawes, G.; Brock, S. L. Control of Phase in Phosphide Nanoparticles Produced by Metal Nanoparticle Transformation: Fe_2P and FeP. *ACS Nano* **2009**, *3*, 2383–2393.
25. Zou, X.; Huang, X.; Goswami, A.; Silva, R.; Sathe, B. R.; Mikmeková, E.; Asefa, T. Cobalt-Embedded Nitrogen-Rich Carbon Nanotubes Efficiently Catalyze Hydrogen Evolution Reaction at All pH Values. *Angew. Chem., Int. Ed.* **2014**, *53*, 4372–4376.
26. Cargnello, M.; Doan-Nguyen, V. V. T.; Gordon, T. R.; Diaz, R. E.; Stach, E. A.; Gorte, R. J.; Fornasiero, P.; Murray, C. B. Control of Metal Nanocrystal Size Reveals Metal-Support Interface Role for Ceria Catalysts. *Science* **2013**, *341*, 771–773.
27. Xiang, Q.; Yu, J.; Jaroniec, M. Synergetic Effect of MoS_2 and Graphene as Cocatalysts for Enhanced Photocatalytic H_2 Production Activity of TiO_2 Nanoparticles. *J. Am. Chem. Soc.* **2012**, *134*, 6575–6578.
28. Wang, C.; Daimon, H.; Onodera, T.; Koda, T.; Sun, S. H. A General Approach to the Size- and Shape-Controlled Synthesis of Platinum Nanoparticles and Their Catalytic Reduction of Oxygen. *Angew. Chem., Int. Ed.* **2008**, *47*, 3588–3591.